Astronomy & Astrophysics manuscript no. qs
October 25, 2010

The brightness of the magnetic field in the quiet Sun

R.S. Schnerr[1,2] and H.C. Spruit[3]

[1] Institute for Solar Physics of the Royal Swedish Academy of Sciences, AlbaNova University Center, SE-106 91 Stockholm
[2] Stockholm Observatory, AlbaNova University Center, SE-106 91 Stockholm, Sweden
[3] Max-Planck-Institut für Astrophysik, Karl-Schwarzschild-Str. 1, D-85748 Garching, Germany

October 25, 2010

ABSTRACT

Context. In addition to the 'facular' brightening of active regions, the quiet Sun also contains a small scale magnetic field with associated brightenings in continuum radiation.
Aims. To measure the contribution of quiet regions to the Sun's brightness, and their possible effect on variations in solar irradiance.
Methods. High spatial resolution (0.″16-0.″32) observations from the Swedish Solar Telescope (SST) and Hinode satellite of the line-of-sight magnetic field and continuum intensity near Fe I 6302.5 Å are used to accurately measure the correlation between field strength and brightness. A detailed model to fit this correlation is developed and applied to calibrate magnetic flux density as a proxy for brightness excess.
Results. In the SST data, the magnetic brightening of a quiet region with an average (unsigned) flux density of 10 G is about 0.15%. The measurement depends on spatial resolution: in the Hinode data, and in SST data reduced to Hinode resolution, the measured brightening is almost a factor 2 lower.
Conclusions. The measured brightness effect is larger than the variation of irradiance over a solar cycle. It is not clear, however, if it constitutes a significant contribution to *variation* of irradiance.

Key words. Sun: surface magnetism – photosphere – solar-terrestrial relations

1. Introduction

The brightness of the Sun is known to vary in phase with the sunspot cycle. In terms of the *total solar irradiance* measured at the (mean) position of the Earth from the Sun (TSI), it is 0.08% brighter at sunspot maximum than at minimum spot activity. The implications of this variation for the Earth's climate are controversial. While a modulation 0.08% on the time scale of the 10-yr cycle does not have significant effects, the effects of possible longer-term variations are still under debate (cf. Foukal et al. 2006). The brightness of the Sun by direct measurement is unknown on time scales longer than the 30 year record of accurate space-based measurements. Because of the close observed correlation between magnetic activity and TSI, it is possible to make an educated guess of the TSI before 1980 by inference from 'proxies': activity indicators like Calcium line emission or the surface magnetic flux, for which longer-term records are available.

The uncertainty in such estimates is that the relation between magnetic fields and their effect on irradiance is not unique. Large flux concentrations (spots and pores) are dark, the small scale field brighter than average, so the mix of small and large has to be known with some accuracy. The brightness of spots is known from observation; that of small scale magnetic concentrations from theoretical models (Spruit 1976, 1977, Spruit & Zwaan 1981) and realistic 3-D radiative MHD simulations (Carlsson et al. 2004, Keller et al. 2004, de Pontieu et al. 2006).

The relative amount of small and large concentrations, however, is variable and presently not predictable from theory or observation. This means that contributions to irradiance have to be considered separately for different kinds of surface magnetic fields. In practice, this is done by classifying areas of magnetic activity into 'spot', 'plage' and 'network' components. Plage and network are quantified using a proxy such as brightness in the Calcium H and K lines. They are spread out over such large areas that their contribution to TSI is below the absolute accuracy of the brightness measurements, and their contributions to TSI cannot be quantified directly. Instead, conversion factors of proxy measurement to TSI contribution are introduced to produce a reconstruction of TSI variation from proxy records, and optimized to obtain a best fit with the measured TSI. In this way, as much as 95% of the TSI variability can be reproduced from known manifestations magnetic activity (Fröhlich & Lean 2004, Wenzler et al. 2006). Within the systematic and statistical accuracy of the data and the proxies used, this value is consistent with 100%, but its significance is subject to the uncertainty introduced by the use of adjustable proxy coefficients.

This fitting process contains uncertainties due to the poorly known contribution from the most uniformly distributed, smallest flux concentrations, near and below current spatial resolution of the observations. At high spatial resolution, the observations show more magnetic flux than at the lower resolution of the standard synoptic magnetograms used for long-term monitoring of solar activity. Especially in the quieter parts of the surface, the small scale magnetic field B tends to be of mixed polarity, which averages out in synoptic maps. A mean 'unsigned' flux density $|B|$ around 10 G appears to be characteristic of areas traditionally called 'quiet' (Lites et al. 2007, 2008). Much of this flux must be in the form of intrinsically weak magnetic fields (compared with the canonical 'kiloGauss fields' in the network boundaries), as shown by their lower center-to-limb variation (Harvey et al. 1975) and the ratio of horizontal-to vertical field strengths (Lites et al. 2008).

Send offprint requests to: R.S. Schnerr, e-mail: roald@astro.su.se

The extent to which magnetic brightening due to this mixed polarity 'quiet Sun' field contributes to irradiance variation is unknown. If this component has a broad distribution over the solar surface, detecting it through a proxy (Ca emission, say) would require the proxy to be measured absolute rather than relative to a background quiet Sun level.

The amount of mixed polarity magnetic field could be used as a proxy for brightness, but in practice this requires very high resolution polarimetric observations. Since full disk monitoring and high resolution observing are mutually rather exclusive, the variation of this component over the activity cycle is not very well known (but see Harvey et al. 1975, Withbroe 2006). It has been suggested before that variations in brightness of the quiet Sun may play an important role in the variation of TSI over a cycle (Ortiz 2004, Withbroe 2006).

2. Measuring the brightness contribution of quiet Sun fields

In high resolution images the brightening of individual magnetic elements can be seen directly in the continuum. Counting these and adding up their excess brightness gives an impression of their contribution to the Sun's overall brightness. Measurements of the magnetic flux contributed by such bright points have been reported by Sanchez Almeida et al. (2010).

Magnetic structure smaller than the resolution of the images escapes detection in such a process based on feature identification. In addition, much of the magnetic structure resides in the dark intergranular lanes. Even when brightened relative to their environment, such structures may still be darker than the mean photosphere, and their contribution is also missed in selection based on brightness. For these reasons, measurements based on feature identification would give only a lower limit to the magnetic brightening. We would like to do better.

2.1. Forward modeling

In the following we develop a method to measure the magnetic brightening of the quiet Sun using the information contained in the distribution of the image data in the $I - B$-plane (brightness vs magnetic flux density). This is done via a model that makes use of a number of known properties of the small scale magnetic field, and fitting this to the observed distribution. With a model thus calibrated the magnetic flux density (average field strength in an image pixel) can also be used as a proxy for the magnetic brightening in the quiet Sun.

2.2. Clues from the correlation between B-field and brightness

An important clue is the run of the average brightness of pixels as a function of their flux density B. Fig. 3 shows that at the low end in B, the brightness first decreases before rising in the more magnetic pixels. The initial decrease is due to the fact that the magnetic field has a tendency to live in intergranular lanes. This is the case both for the intrinsically weak ($\ll$kG) and strong ('flux tube') magnetic fields. The precise shape of this curve can be used to determine the relative amount of weak and strong field, and the brightness excess of the strong fields as a function of apparent flux density in the image. As described in more detail in Sect. 5, this allows the small brightness increase due to magnetic field to be constructed reliably from the data.

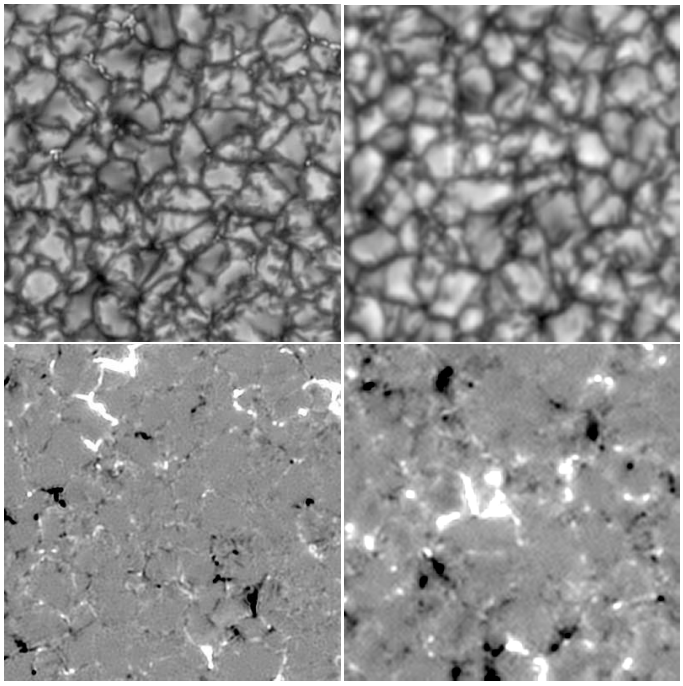

Fig. 1. Quiet regions at disk center as seen in continuum around 630.5 nm and in magnetic flux density, showing 20″x 20″subfields of the SST (left) and Hinode (right) observations used. Flux density range is from -100 (black) to 100 G (white)

3. Observations

We investigate two disk center quiet Sun fields; one observed with the imaging spectropolarimeter CRISP (Scharmer 2008) on the Swedish Solar Telescope (SST) and one with the Spectropolarimeter (SP) on the Solar Optical Telescope (SOT) of Hinode (see Fig. 1). The SST observations, obtained on the 23rd of May 2009, cover the 6302.5 Å Fe I spectral line, have a pixel scale of 0.″0592 and cover a 1024x1024 field. This gives a total field-of-view of about 60″x60″. The data cover 11 wavelengths, of which three in a telluric line and one continuum point. Inversions were performed with a parallelized version of the inversion code Nicole (Socas-Navarro et al. 2010).

The Hinode observations, taken on the 10th of March 2007, cover both the 6301.5 and 6302.5Å Fe I line, have a pixel scale of 0.″16 and a total (scanned) field-of-view of 164″x328″. The magnetic field data were taken from the level 2 data products available online[1]. Magnetic field strengths have been converted to fluxes by taking the filling factor into account. This field has already been described by Lites et al. (2008).

The diffraction limits of SST and Hinode satellite at 6302 Å are 0.″16 and 0.″32, respectively. The average flux density in the Hinode field is 10.8 G, in the SST field 10.1 G. This includes corrections for the measurement noise in the magnetic field. The corrections are small, of order 1 G, because most of the flux appears in fields stronger than the measurement noise.

Since the SST field has a higher resolution than the Hinode data (cf. Fig. 1), the flux numbers cannot be compared directly. When convolved to the Hinode resolution, the average unsigned flux density in the SST data drops by 15%, to 8.5 G (see Sect. 6.2.1 for more on this comparison).

[1] http://sot.lmsal.com/data/sot/level2dd

4. Weak fields and strong fields

The observed correlation of the Sun's brightness with the small scale magnetic field is understood as a consequence of the local change in radiative energy transfer in the surface layers caused by the magnetic fields (the lower opacity inside the field due to magnetic pressure, Spruit 1976, 1977). The effect has been reproduced in impressive detail in realistic 3-D magnetohydrodynamic simulations (Carlsson et al. 2004, Keller et al. 2004, see also Steiner 2005, de Pontieu et al. 2006). Since the effect scales with the magnetic pressure $B^2/8\pi$, intrinsically strong fields (the kG 'flux tubes') have a stronger effect on brightness, per unit of magnetic flux, than intrinsically weak fields. To use magnetic flux as a proxy for brightness, it is thus necessary to separate the contributions of intrinsically weak and strong fields.

Intrinsically weak fields are seen on the surface in the form of the so-called *inner network fields* (Livingston & Harvey 1975, Harvey et al. 1975). Their magnetic signal does not show a strong center-to-limb variation, indicating that their orientation is more or less isotropic. This is in contrast with the strong 'kG-fields', which show a characteristic decline of their Stokes-V signal towards the limb (Martin & Harvey 1979). This means that strong fields are nearly vertical to the surface, as expected from their magnetic buoyancy (e.g. Meyer et al. 1979).

Whereas the strong fields are highly concentrated in the intergranular lanes, the weak fields are somewhat more uniformly distributed. They are advected towards granulation and intergranulation boundaries as expected from a weak magnetic field, but their short life time is compensated by continued emergence inside granular and intergranule cells (Martin 1988). Phenomena much like those observed have been reproduced in realistic 3−D MHD simulations by Schüssler & Vögler (2008). These results indicate that local near-surface dynamo action, independent of the solar cycle, may be responsible for the observed weak fields.

5. Model

From the above it is clear that a model for the distribution of magnetic fields and their brightness contribution needs to take into account the different properties of a weak field and a strong field component. The intrinsically weak component: a) does not contribute to excess brightness, and b) is distributed more uniformly than the strong component. The strong component a) has a brightness excess with respect to its surroundings, and b) is distributed mainly in the intergranular lanes.

We take these properties into account in the following way. The fraction of pixels f_B with a given flux density B is taken from the observations to be fitted. We divide f_B into an intrinsically weak fraction $f_{\rm w}(B)$ and an intrinsically strong fraction $1 - f_{\rm w}$. The number of pixels assigned to the weak and strong fractions are thus:

$$n_{\rm w}(B) = n f_B f_{\rm w}, \qquad n_{\rm s}(B) = n f_B (1 - f_{\rm w}), \tag{1}$$

where n is the total number of pixels. For the dependence of $f_{\rm w}$ on B we take a smooth transition:

$$f_{\rm w} = e^{-B/B_c}, \tag{2}$$

where B_c is one of the model parameters to be fitted to the data.

The brightness excess of the modeled fields is described by assigning them contrast $q(B_0)$ with respect to their surroundings, where B_0 is the intrinsic field strength of the magnetic element (as opposed to the measured average flux density B in a pixel). If I, $I_{\rm b}$ are the brightness of the field element and that of the surroundings in which it is embedded,

$$I = [1 + q(B_0)] I_{\rm b}. \tag{3}$$

For the weak field component, the model assumption is simply $q_{\rm w} = 0$, while the strong field will be given a nonzero brightness contrast. Ideally this should be a function of the size of the magnetic element, since small elements ($\lesssim 0\farcs5$) produce a larger brightness excess than larger ones ('pores'). In the larger ones the center becomes dark, as seen in the observations (e.g. Spruit and Zwaan 1981) and reproduced in 3-D MHD simulations (Carlsson et al. 2004, de Pontieu et al. 2006). Contrast $q_w(B_0)$ would thus be a declining function of size, becoming negative in areas with large concentrations of magnetic flux.

The intrinsic field strength can be retrieved from the data only in sufficiently well resolved structures, however. At the small sizes that have the largest brightness contribution per unit magnetic flux the structures are not resolved at even the best telescope resolution, while their arbitrary location in the image means that most pixels will cover only a part of the structure. At low magnetic flux, we therefore interpret the observed flux density as reflecting *filling factor*. The contrast of these pixels is taken proportional to the filling factor or the observed flux density B. Together with the observed brightness decline at large flux density, we represent this by the following simple quadratic dependence of the model contrast $q_{\rm s}$ of the strong field component on the observed flux density:

$$q_{\rm s}(B) = aB\left(1 - \frac{B}{2B_{\rm m}}\right), \tag{4}$$

where $B_{\rm m}$ is the flux density where brightness contrast peaks, and a an amplitude factor. Both are fitting parameters of the model. At low B, the contrast described by Eq. (4) is linear in B, $q_{\rm s} \approx aB$, and a is the brightness excess 'per Gauss of flux density'.

The precise shape of the 'hooklet' in Fig. 3: the initial steep decline of mean brightness with increasing field flux density B and its subsequent gradual rise, depend critically on the way the magnetic fields are distributed in the granulation pattern. The initial decline shows that the weak field component, from being almost uniformly distributed at very low flux density, with increasing field strength favors the darker intergranular lanes. Since the weak component has little contrast relative to its surroundings, magnetic pixels at low flux density are darker than average.

The intrinsically strong component has a positive contrast relative to its intergranular surroundings, but at low filling factor the darkness of its surroundings dominates. Though darker than the average photosphere, they still make a positive contribution to the brightness of the area, because they are brighter than the intergranular lane would have been without them.

The model has to fit not just the mean brightness $\bar{I}(B)$ as a function of flux density, but also the distribution of brightness in the entire $I - B$ plane. For this, probability distributions $p(I_{\rm b}, B)$ are needed for the brightness $I_{\rm b}(B)$ of the surroundings of the magnetic elements. We call $p(I_{\rm b}, B)$ the 'background' brightness distribution. At zero magnetic flux this is the distribution of brightness I_0 of the non-magnetic Sun,

$$p_0 \equiv p(I, B = 0). \tag{5}$$

We measure it from the image as the brightness distribution of pixels with magnetic flux less than the measurement noise. In units of the average brightness $\langle I_0 \rangle$ of the nonmagnetic surface,

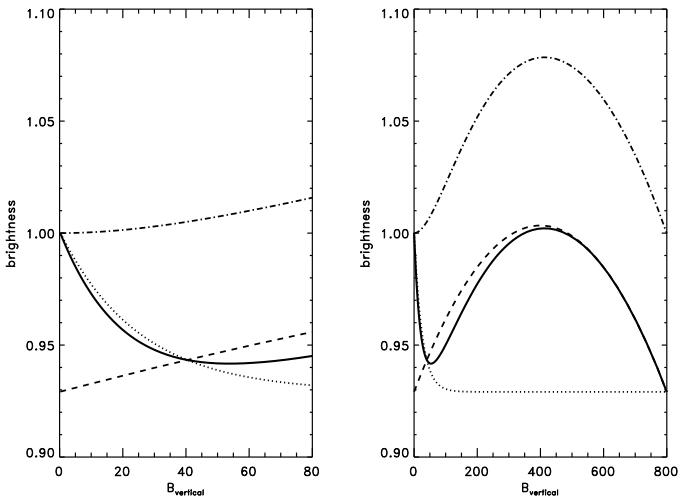

Fig. 2. Effect of the different ingredients of the model. Solid: model fit of the brightness as function of observed flux density B (the dotted line in Fig. 3, Hinode data). Dotted: same if the bright strong field component is omitted from the model. Dashed: same if the weak field component is omitted. Dot-dashed: predicted magnetic brightness if the preference for intergranular lanes were absent.

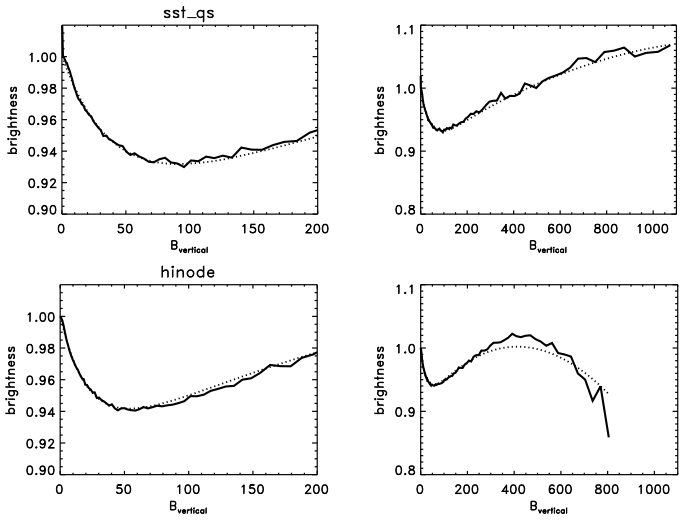

Fig. 3. Solid: mean brightness as a function of flux density in the SST (top), and the Hinode (bottom) quiet Sun fields. Dotted: model fits

I_b ranges from a minimum $I_1 \approx 0.8$ to a maximum $I_2 \approx 1.2$. The distribution of brightness in the intergranular lanes where most of the flux resides is not known a priori and must instead be found by fitting to the observed distribution of points in the $I-B$-plane. We find that a suitable starting guess is a 'squeezed' version of p_0:

$$\begin{aligned} p_\mathrm{ig}(I) = \; & p_0\left(I_1 + (I-I_1)\tfrac{I_2-I_1}{I_\mathrm{ig}-I_1}\right) && (I_1 < I < I_\mathrm{ig}), \\ = \; & 0 && (I > I_\mathrm{ig}). \end{aligned} \tag{6}$$

where I_ig ($< I_2$) is a fitting parameter, a measure of the maximum brightness of the intergranular surroundings of the magnetic fields.

For the dependence of $p(I,B)$ on observed flux density B, a simple exponential for the transition between p_0 and p_ig turns out to provide a good fit to the data:

$$p(I,B) = p_0 e^{-B/B_w} + p_\mathrm{ig}(1-e^{-B/B_w}), \tag{7}$$

were B_w is a model parameter determining the width of the transition.

Not counting quantities like p_0 which have been measured from the data itself, the model thus has 5 parameters: $B_\mathrm{w}, B_\mathrm{c}, B_\mathrm{m}, a, I_\mathrm{ig}$.

The effect of the different ingredients of the model are shown in Fig. 2. It shows the model fit (solid line) for the parameter values that fit the Hinode data. The dot-dashed line shows the model prediction if the preference of magnetic fields for intergranular lanes is left out of the model. The dotted line shows how the initial decline of brightness with flux density is due to the increasing tendency of the weak field component to live in the intergranular lanes.

6. Results

6.1. Fits to the data

Figure 3 shows the dependence of average brightness $\bar{I}(B)$ as a function of flux density for the SST and Hinode quiet Sun fields, together with the model fits. For the SST data, the fit yields $B_\mathrm{w} = 80$ G, $B_\mathrm{c} = 100$ G, $B_\mathrm{m} = 1500$ G, $a = 4.5\,10^{-4}$ G^{-1}, $I_\mathrm{ig} = 1.01$, for the Hinode data $B_\mathrm{w} = 25$ G, $B_\mathrm{c} = 100$ G, $B_\mathrm{m} = 400$ G, $a = 4.0\,10^{-4}$ G^{-1}, $I_\mathrm{ig} = 1.08$. At low flux density (left panels) the two fields are similar, but at higher flux density the Hinode field contains relatively more dark structures (pores) than the SST field.

The slope of the initial decline of I with B is controlled mostly by the value of B_z. B_c determines the location of the minimum of the curve, I_ig the brightness level of this minimum, B_m the location of the maximum and a the brightness level at maximum. Thus 5 is the minimum number of parameters needed for a fit, and since a good fit is obtained with the 5 parameters used, there is no justification for additional parameters.

The model also provides a good fit to the distribution of points in the I-B-plane, with these parameter values. At low B the fit is exact (by construction, because of the use of I_0 from the data itself). At higher B, the model distribution $p(I)$ is a bit narrower than the observations. Experiments with somewhat wider distributions showed that the results depend only marginally on this part of the fitting process, however.

6.2. Brightness effect

From the model fits, the excess brightness contribution of the magnetic field can now be computed. Let $n_i(B)$ be the number of pixels in bin i with flux density B_i, $n = \Sigma_i n_i$ the total number of pixels, $q(B_i)$ the contrast of the strong field component at this flux density (cf. Eq. (4)), and $f_\mathrm{s} = 1 - f_\mathrm{w}$ the fraction of these pixels that are in the strong field component. The cumulative brightness effect $\delta I(B)$, i.e. the effect contributed by all pixels with flux density less than B, is given by

$$\delta I(B_i) = \frac{1}{n}\Sigma_{j<i}\, n_j f_\mathrm{s}(B_j) q(B_j). \tag{8}$$

The result is seen in Fig. 4, which shows the cumulative distribution of excess brightness as a function of flux density. Integrated over all pixels, the effect is of the order 0.1%, while pixels with flux density less than 50G still contribute about 0.03%. The effect is somewhat larger in the SST region than in the Hinode observation. Since the SST data have a higher spatial resolution

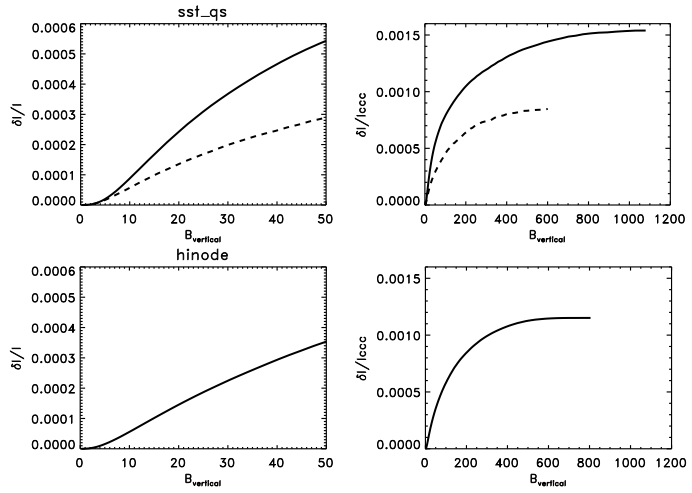

Fig. 4. Cumulative brightness effect: excess contributed by all pixels with flux density less than B, as function of B. The dashed lines in the top panels show the effect of smearing the SST data to the Hinode resolution and pixel scale.

than the Hinode data (cf. Fig. 1), however, the brightness effect of the two cannot be compared directly.

6.2.1. Dependence on resolution

To investigate the effect of spatial resolution on the result shown in Fig. 4, we have repeated the analysis on the SST data after convolving them to a spatial resolution comparable with the Hinode data. The Hinode point spread function has been measured by Mathew et al. (2009, see also Wedemeyer-Böhm 2008). At 6300 Å, its Gaussian core has a width (standard deviation) of 0.″21 (i.e. FWHM of ≈ 0.″4).

Instead of this value, we have convolved our SST data with a somewhat narrower Gaussian, of width 0.″15 (roughly 3 SST pixels), and the result rebinned to the Hinode pixel scale of 0.″16. The convolution width of 0.″15 was chosen such as to yield an rms contrast equal to that of the Hinode image (7.4%). This is the most relevant measure for comparing our data with the Hinode image, since the brightness contrast of small structures is just the effect we are measuring in this study, and makes the comparison independent of uncertainties in the actual point spread functions of the Hinode and the SST data.

This smearing + rebinning process reduces the average flux density from 10.1 G to 8.5 G. At the same spatial resolution, the SST field is thus actually a bit quieter than the Hinode field (10.8 G). Repeating the analysis on these reduced-resolution data gives the dashed curves in Fig. 4. The corresponding values of the fitting parameters are now $B_\mathrm{w} = 35$ G, $B_\mathrm{c} = 100$ G, $B_\mathrm{m} = 600$ G, $a = 4.0\,10^{-4}$ G^{-1}, $I_\mathrm{ig} = 1.05$. These numbers, as well as the brightness curve itself, are now rather close to those determined from the Hinode data.

The net brightness effect deduced for the area as a whole has decreased significantly by the reduced resolution, from $\delta I/I = 1.5\,10^{-3}$ to $0.85\,10^{-3}$. Within the systematic uncertainties, the remaining difference in net brightening compared with the Hinode data ($\delta I/I = 1.15\,10^{-3}$) is accounted for by the lower average flux density in the SST area.

7. Discussion and conclusions

Analyzing two regions of quiet Sun with data from the Swedish 1m Solar Telescope and SOT on the Hinode satellite we find that the mixed polarity magnetic field in the quiet Sun contributes a brightening of about 0.15% at disk center at $\lambda = 6300$ Å. This is more than the variation of total solar irradiance over a solar cycle.

The method developed here uses the information contained in the dependence of brightness on magnetic flux density as measured from the distribution of image pixels in the I (continuum brightness) vs. B (unsigned flux density) plane. It requires the use of some external information, such as observed properties of the 'intrinsically weak' field component (discussed below) but does not suffer selection effects, capturing contributions that would be missed by feature identification-based approaches. As a byproduct, it also provides information on amplitude and distribution of the weak field component.

The observations are sensitive only to the average magnetic flux in a resolution element of the observation, not the intrinsic field strength (at least not at the low flux levels considered), so this distinction cannot be made individually per pixel, but only in a statistical sense. We have shown how a statistical assessment is possible using the characteristic shape of mean brightness as a function of flux density (Fig. 3).

An important aspect of this analysis is the distinction between strong, 'kilogauss' fields and the intrinsically weak, predominantly horizontal magnetic field component in quiet regions (Martin & Harvey 1979, Lites et al. 2008). Since the thermodynamic effects of a magnetic field scale as B^2, the intrinsically weak component is expected to contribute little to changes in brightness, but significantly to the average flux density in the quiet Sun. The model takes this into account by fitting a mixture of the weak and intrinsically strong components, assuming zero intensity contrast for the weak component.

The results show that spatial resolution has a significant effect on the detectability of magnetic brightening. The brightening of the SST region analyzed drops by almost a factor 2 when the resolution is reduced to that of the Hinode data.

The mean unsigned flux levels for quiet Sun reported so far, including our SST data, have consistently been around 10 G, suggesting a fairly stable quiet Sun level. More systematic measurements in quiet areas, in time and in position on Sun would be needed to confirm this. Because of projection effects, the intrinsically strong component of the small scale field is visible especially towards disk center (towards the limb the brightness effect is dominated by 'faculae', consisting of larger flux concentrations, Spruit 1976).

The brightness effect measured is monochromatic at 6302 Å; the contributions at other wavelengths would need to be considered as well for a more quantitative estimate of the effect on solar irradiance (TSI).

7.1. Strong fields from weak fields?

The intrinsically weak field component, on theoretical grounds assumed here to have negligible continuum intensity contrast, are not in themselves of interest for the main question addressed. It is gratifying, however, that the results reported here agree qualitatively with the findings from numerical simulations (Schüssler & Vögler 2008, Pietarila Graham et al. 2009). In these simulations, the advection and subsequent compression of weak fields into the intergranular lanes generated field strength up to kG values. This raises the possibility that a part of the intrinsically

strong field identified in our analysis actually represents this weak field dynamo process rather solar-cycle related mixed polarity fields.

7.2. Contribution to TSI variation?

Whether the brightness effect found here is of importance for solar irradiance depends on the degree to which it varies, especially on the time scale of the solar cycle or longer. It is not obvious that the increase of 0.15% over a hypothetical field-free Sun, though of the same magnitude as the variation of TSI over a cycle, has much practical effect since the Sun is not observed to be field-free even at minimum activity.

If the strong field component of the mixed polarity flux in quiet Sun is in actually part of a weak-field dynamo process, it is expected to be independent of the solar cycle. The brightness-relevant fields in quiet Sun measured here would then be stable in time, making them irrelevant for TSI variations. On the other hand, it is known from synoptic data that simple decay of active regions by dispersal of its magnetic flux contributes directly to the quiet Sun as seen for example in the Calcium network. In addition, a large amount of short-lived magnetic flux appears in the form of ephemeral active regions (Harvey et al. 1975). There must thus also be a contribution to the quiet Sun magnetic field that depends on the solar cycle.

Not addressed in all of the above is the possibility of secondary effects of magnetic fields on brightness: effects that would be due to the presence of the field, but not strictly cospatial with it. Potentially most worrying of these is the effect of strong magnetic flux bundles on the pattern of convection around them. Minor effects on convective transport efficiency due to embedded flux bundles, too low to be measured directly on the Sun or in simulations, might still be large enough to have a noticeable net brightness effect. Such effects are taken into account implicitly in proxy data calibrated against observed TSI variation, but one would still feel more comfortable if a more direct assessment of their effect could be made.

Acknowledgements. R.S. would like to thank C.E. Fischer. The Swedish 1-m Solar Telescope is operated on the island of La Palma by the Institute for Solar Physics of the Royal Swedish Academy of Sciences in the Spanish Observatorio del Roque de los Muchachos of the Instituto de Astrofísica de Canarias. Hinode is a Japanese mission developed and launched by ISAS/JAXA, with NAOJ as domestic partner and NASA and STFC (UK) as international partners. It is operated by these agencies in co-operation with ESA and NSC (Norway).

References

Carlsson, M., Stein, R. F., Nordlund, Å., & Scharmer, G. B. 2004, ApJ, 610, L137
De Pontieu, B., Carlsson, M., Stein, R., et al. 2006, ApJ, 646, 1405
Foukal, P., Fröhlich, C., Spruit, H., & Wigley, T. M. L. 2006, Nature, 443, 161
Fröhlich, C., & Lean, J. 2004, A&A Rev., 12, 273
Harvey, K. L., Harvey, J. W., & Martin, S. F. 1975, Sol. Phys., 40, 87
Keller, C. U., Schüssler, M., Vögler, A., & Zakharov, V. 2004, ApJ, 607, L59
Lites, B., Socas-Navarro, H., Kubo, M., et al. 2007, PASJ, 59, 571
Lites, B. W., Kubo, M., Socas-Navarro, H., et al. 2008, ApJ, 672, 1237
Livingston, W. C., & Harvey, J.W. 1975, BAAS, 7, 346
Martin, S. F., & Harvey, K. H. 1979, Sol. Phys., 64, 93
Martin, S. F. 1988, Sol. Phys., 117, 243
Mathew, S.K., Zakharov, V. & Solanki, S. 2009, A&A501, L19
Meyer, F., Schmidt, H. U., Simon, G. W., & Weiss, N. O. 1979, A&A, 76, 35
Ortiz, A. 2004, 35th COSPAR Scientific Assembly, 35, 492
Pauluhn, A., & Solanki, S. K. 2002, SOLMAG 2002. Proceedings of the Magnetic Coupling of the Solar Atmosphere Euroconference, 505, 521
Pietarila Graham, J., Danilovic, S., & Schüssler, M. 2009, ApJ, 693, 1728
Sánchez Almeida, J., Bonet, J. A., Viticchié, B., & Del Moro, D. 2010, ApJ, 715, L26
Scharmer, G. B., Narayan, G., Hillberg, T., et al. 2008, ApJ, 689, L69
Schüssler, M., & Vögler, A. 2008, A&A481, L5
Socas-Navarro, H., de la Cruz Rodríguez, J., Asensio-Ramos, A., Trujillo-Bueno, J., & Ruiz-Cobo, B. 2010, in prep.
Spruit, H. C. 1976, Sol. Phys., 50, 269
Spruit, H. C. 1977, Sol. Phys., 55, 3
Spruit, H. C., & Zwaan, C. 1981, Sol. Phys., 70, 207
Steiner, O. 2005, A&A, 430, 691
Wedemeyer-Böhm, S. 2008, A&A, 487, 399
Wenzler, T., Solanki, S. K., Krivova, N. A., & Fröhlich, C. 2006, A&A, 460, 583
Withbroe, G. L. 2006, Sol. Phys., 235, 369